

1 **Constraining spatio-temporal characteristics of magma**
 2 **migration at Piton de la Fournaise volcano from pre-eruptive**
 3 **seismicity**

4 **Z. Duputel¹, O. Lengliné¹ and V. Ferrazzini²**

5 ¹Institut de Physique du Globe de Strasbourg, UMR7516, Université de Strasbourg/EOST, CNRS, Strasbourg,
 6 France.

7 ²Observatoire Volcanologique du Piton de la Fournaise, Institut de Physique du Globe de Paris, Sorbonne
 8 Paris Cité, Univ. Paris Diderot, CNRS, F-97418, La Plaine des Cafres, La Réunion, France.

9 **Key Points:**

- 10 • We use a template matching technique to detect and relocate earthquakes during the
 11 13 last eruptive unrests at Piton de la Fournaise volcano
- 12 • Almost all detected events are located on a ring-shaped structure, corresponding to
 13 an area of weakness in the upper edifice of the volcano
- 14 • The location and timing of pre-eruptive seismic swarms on this ring-shaped struc-
 15 ture bring information on the future eruptive site

16 **Abstract**

17 Volcano-tectonic seismicity has been recorded for decades on various volcanoes, and is
 18 linked with the magma transport and reservoir pressurization. Yet, earthquakes often ap-
 19 pear broadly distributed such that magma movement is difficult to infer from its analysis.
 20 We explore the seismicity that occurred before eruptions at Piton de la Fournaise in the
 21 last 5 years. Using template matching and relocation techniques, we produce a refined
 22 image of the summit seismicity, demonstrating that most earthquakes are located on a
 23 ring structure. However, only a portion of this structure is activated before each eruption,
 24 which provides an indication as to the direction of the future eruptive site. Furthermore,
 25 we show that the delay between the pre-eruptive swarm and the the eruption onset is pro-
 26 portional to the distance of the eruptive fissures relative to the summit cone. This reveals
 27 that the beginning of the intrusion already bears information regarding the future eruption
 28 location.

29 Plain Language Summary

30 Earthquakes on volcanoes are usually related to the ascent of magma in the edifice and
31 can therefore provide information concerning an impending eruption. Yet on many occa-
32 sions, it is not easy to relate the recorded seismicity to the propagation of magma in the
33 volcano. In this study, we detect and locate earthquakes that occurred before 13 eruptions
34 at Piton de la Fournaise, a hawaiian-type volcano located on La Réunion island in the In-
35 dian Ocean. We demonstrate that a detailed analysis of the seismicity occurring when the
36 magma starts its ascent can bring important information regarding the future eruption lo-
37 cation.

38 Keywords

39 Volcano seismicity; Magma migration; Piton de la Fournaise; Template matching

40 **1 Introduction**

41 One goal of volcano monitoring is to provide reliable information concerning an
 42 impending eruption. With this purpose, one generally relies on the detection of anomalous
 43 signals that could reflect magma intrusions within the edifice. A major challenge is
 44 the difficulty in interpreting the different observations that are recorded during the pre-
 45 eruptive phase. Volcano-tectonic events are often considered to signal dynamic shear fail-
 46 ure within the edifice. It is envisioned that a migrating magma pressure source can lo-
 47 cally create high-stress concentrations that ultimately result in material failure and micro-
 48 earthquakes. Such a relation between the propagation of a magma-filled dike and the oc-
 49 currence of earthquakes has been documented on several occasions [e.g. *Einarsson and*
 50 *Brandsdóttir*, 1980; *Rubin et al.*, 1998; *Battaglia et al.*, 2005; *Grandin et al.*, 2011; *Sig-*
 51 *mundsson et al.*, 2015]. However, it is often not easy to relate the recorded seismicity to
 52 a moving magma source. In certain circumstances, a dike can even intrude the volcanic
 53 edifice with no detectable earthquakes [e.g., *Aki and Koyanagi*, 1981; *Wright et al.*, 2006].
 54 Indeed, as noted by *Rubin and Gillard* [1998], the occurrence of earthquakes large enough
 55 to be detected most likely corresponds to the failure of pre-existing weak structures within
 56 the edifice in the vicinity of the propagating crack, but not necessarily the exact tip of the
 57 dike. Furthermore, the final stage of the magma ascent is often accompanied by very low
 58 seismic activity only comprising low amplitude events that are difficult to track and lo-
 59 cate [*Taisne et al.*, 2011; *Zecevic et al.*, 2013; *Eibl et al.*, 2017]. This is because the low
 60 stresses at shallow depth only permit very small earthquakes that cannot be easily detected
 61 and located. In addition, upper parts of volcanic edifices are usually highly heterogeneous,
 62 which can prevent long faults to develop. Therefore, as shallow magma chambers are usu-
 63 ally found on basaltic volcanoes, the last stage of magma propagation between such reser-
 64 voirs and the surface is difficult to track. It thus limits our ability to make predictions of
 65 the future surface eruptive activity based on seismicity recording.

66 In this study, we focus on the Piton de la Fournaise volcano located on La Réunion
 67 island in the Indian Ocean. This frequently-active (i.e., 13 eruptions between June 2014
 68 and July 2018; Table 1) basaltic volcano represents an excellent field laboratory that is
 69 monitored by a dense network of geodetic and seismological stations [see Fig. 1; *Bren-*
 70 *guier et al.*, 2012; *Staudacher and Peltier*, 2016]. Being able to predict the location of a
 71 future eruption is of great interest at the Piton de la Fournaise. Indeed, a major concern
 72 are distal flank eruptions close to inhabited areas outside of the Enclos Fouqué caldera. In

addition, as the volcano is a popular tourist attraction [with over 350 000 visitors per year; *Harris et al.*, 2017], the prediction of eruptive fissure location is important to plan the evacuation of visitors hiking into the caldera. Eruptions are generally preceded by an intense shallow seismic crisis lasting a few hours [*Roult et al.*, 2012], which originates from a persistent structure located below the volcano summit around sea level [*Sapin et al.*, 1996; *Lengliné et al.*, 2016]. Some shallow events are occasionally captured in the latter stage of the crisis but they are usually difficult to locate [e.g. *Taisne et al.*, 2011; *De Barros et al.*, 2013]. In fact, most events located before eruptions remain confined below the central cone and do not track the last stage of magma movement. Here, we use a template matching technique to detect and relocate seismic events during the 13 last eruptive unrests at Piton de la Fournaise volcano. We show that a careful analysis of the pre-eruptive seismicity provides clear indications as to the location of an oncoming eruption.

2 Data and Methods

Earthquake detection is conducted using a template matching procedure following the same approach described in *Lengliné et al.* [2016]. This detection process has been directly implemented at the Piton de la Fournaise Volcano Observatory (OVPF) to provide an automated detection of any seismic events. Each day, we build a template earthquake catalog from the last 1000 events manually located in the shallow part of the volcano. Among these 1000 template candidates, we only select events that have a depth uncertainty lower than 340 m and be located above sea level in the Enclos Fouqué caldera. We then scan the previous 24 hours of continuous seismic data to detect events that match at least one of the events in this template list. The earthquake detection is performed using the vertical components of at least 3 stations near the central cone (BOR, BON, SNE, FJS, RVL or CSS). All traces are filtered between 5 and 25 Hz. For each template, we compute correlation coefficients for each time-step (0.01 s) on all selected channels. We then apply a maximum filter over a duration of ± 0.1 s and stack the correlation traces after applying a travel-time correction. We consider all time-windows where the average correlation over the last three traces is larger than 0.45 as possible detections. In the case when multiple templates lead to a common detection, we only consider the detection associated with the template that produced the highest correlation coefficient with the continuous data stream. Once detection times have been obtained, we extract the waveforms at all of the stations in the OVPF network for each newly detected event based on the template travel

105 times. This results in a total set of 16 246 events between June 2014 and July 2018. This
 106 compares to the 1635 events that are listed in the original catalog for the same time pe-
 107 riod. Almost all of these events occur during the seismic crises that precede the eruptions
 108 listed in Table 1.

109 In order to obtain the precise location of each event, we use a double-difference rel-
 110 ative location algorithm [Waldfhauser, 2000]. We first compute P- and S-wave differential
 111 travel times for all pairs of detected events on 1.28 s long windows based on the maxi-
 112 mum of the cross-correlation function. The differential travel times of P-wave are com-
 113 puted on vertical components whereas the differential travel times of S-waves are obtained
 114 on both horizontal components. Following *Carrier and Got* [2014], we apply an *a priori*
 115 Cauchy distribution with $\sigma_0=0.1$ s to this cross-correlation function in order to mitigate
 116 the contamination of outliers in the dataset. We discard travel time delays when the cor-
 117 relation coefficient multiplied by the *a priori* function is lower than 50%. All events are
 118 finally relocated together which results in a final set of 15 598 relocated events. We use
 119 a simple homogeneous velocity model for the relocation with a P-wave velocity of 3.0
 120 km.s⁻¹, a V_P/V_S ratio of 1.73. We also account for the station elevations when computing
 121 ray paths. Events that are discarded during the relocation process correspond to earth-
 122 quakes that have too few links with other events to be adequately relocated.

123 3 Results

124 The entire set of relocated earthquakes is presented in Fig. 1. We observe that al-
 125 most all events focus on a ring structure located below the summit of the volcano be-
 126 tween a depth of 200 m and 1 km above sea level. This structure was already evidenced by
 127 *Lengliné et al.* [2016] using data from the 2014 and 2015 eruptions. It delineates a persis-
 128 tent feature of the volcanic edifice with a dip of 20° towards the east (Fig. 1). Its location
 129 is considered to correspond to a zone of weakness or stress concentration at the roof of
 130 the magma reservoir [located around sea level according to previous studies; *Peltier et al.*,
 131 2005; *Lénat et al.*, 2012]. Our updated relocated catalog seems to show more details than
 132 previous studies [e.g., *Sapin et al.*, 1996; *Lengliné et al.*, 2016]: we notice secondary seis-
 133 micity alignments inside the main ring structure such as a N45° lineation that is clearly
 134 visible to the north-east of the Dolomieu crater in Fig. 1b. This structure certainly cor-
 135 responds to a ring fault system hosting repetitive collapses of the volcano summit [e.g.,
 136 *Staudacher*, 2010]. Alignments of seismicity inside the main ring structure might outline

secondary faults or weak structures associated with the different collapsed areas that affected Dolomieu and Bory summit craters in the past [Michon *et al.*, 2013]. Earthquake swarms that occur on the ring structure before each eruption seem to have distinct locations. Indeed, the correlation matrix highlighting the similarity of the recorded signals shows that events are mostly correlated with earthquakes belonging to the same pre-eruptive swarm (cf., Fig. S1 in the supporting information). One consequence of this poor correlation among seismic swarms is that most earthquakes are detected shortly before or after their template events (cf., Fig. S2).

To analyze the pre-eruptive activity, we focus on events that occurred within 24 hours before each of the 13 eruptions that occurred between 2014 and 2018 (see Table 1). Eruptions at Piton de la Fournaise are typically preceded by a seismic crisis a few hours before the eruption onset. We report in Fig. 2 the location of earthquakes preceding each eruption along with the corresponding eruptive fissures. For all eruptions, we readily observe that only a portion of the ring structure is activated during the pre-eruptive seismic crisis. Furthermore, we clearly see that the activated portion of the ring provides a good indication of the future eruptive fissure location. More specifically, the azimuth of the eruptive site relative to the summit area can be extrapolated from the location of earthquakes on the main ring structure. We can see in Fig. 2, Fig. S3 and Fig. S4 that we have a perfect match for all 13 analyzed eruptions. It suggests that, although individual events do not allow us to track the magma propagation all the way up to the surface, there is a clear link between earthquake locations on the ring structure and the existence of a moving magma body.

To investigate how the pre-eruptive seismicity is connected to the mass magma transport within the edifice, we measure the timing of the seismic crises relative to the eruption onsets. Pre-eruptive seismic crises are conspicuous on the seismograms presented in Fig. 3: eruptions are systematically preceded by a significant increase of seismicity for a duration that varies significantly between each eruption (from a few tens of minutes to more than 8 hours). We can also note that the earthquake rate drops before the onset of the eruptions. As mentioned before, this suggests that the ultimate propagation of the magma up to the eruptive site is mostly aseismic, which makes it difficult to track using earthquakes. Some events can still be detected during this phase (see Fig. 2) but they are difficult to locate because they are usually visible only at a few stations [e.g Taisne *et al.*, 2011; De Barros *et al.*, 2013]. We can however investigate if there is any relationship be-

tween the timing of the seismic swarms and the location of the eruptive sites. Fig. 3 shows the pre-eruptive time-delay of the seismic swarms as a function of their distance to the eruption sites. Pre-eruptive time-delays correspond to the time difference between the beginning of the seismic crisis and the eruption onset. They are computed using a simple approach, considering that the seismic crisis starts when the earthquakes rate reaches a threshold of 150 events per hour. The distance to the eruption site is defined as the shortest distance between earthquakes occurring at the beginning of the seismic crisis and the eruptive fissures. There is a clear correlation between the time-delay and the distance of the seismic swarms to the eruption sites. This simply indicates that an eruption occurring at a large distance from the magma reservoir will also occur at a large delay after the onset of the seismic crisis. This is consistent with previous studies showing that longer seismic crisis are usually associated with eruptions at larger distances from the summit [Aki and Ferrazzini, 2000; Peltier et al., 2005; Roult et al., 2012]. A rough linear fit on the observed scaling allows us to constrain a migration speed for the magma of the order of 0.1 m.s⁻¹.

4 Discussion

Seismicity is not always a straightforward indicator of magma propagation. Although volcano-tectonic earthquakes can sometimes be interpreted as a direct marker of dike pathways [e.g., Rubin et al., 1998; Sigmundsson et al., 2015], it can also correspond to distributed damage caused by pressure variations in the magma reservoir [Carrier et al., 2015] or alternatively as the result of pre-existing suitably oriented structures already near to failure [Rubin and Gillard, 1998]. At Piton de la Fournaise, almost all pre-eruptive seismicity is focused on the same ~20° eastward dipping ring-shaped cluster below the summit and above a shallow magma reservoir located around sea level [see Fig. 1; Peltier et al., 2009]. This cluster certainly represent an area of weakness outlining the piston structure associated with the repetitive formation of pit craters and caldera collapses in the volcano summit [Michon et al., 2013; Lénat et al., 2012]. This interpretation seems consistent with the existence of a shallow low-density fractured column beneath the central cone that has been inferred from gravity measurements [Gaillet et al., 2009]. Such a weakened zone that is prone to failure can facilitate the propagation of magma intrusions. These intrusions can in turn maintain damages within the edifice due to the associ-

201 ated stress changes and induced hydrothermal alteration §[*Pola et al.*, 2012; *Wyering et al.*,
 202 2014; *Heap et al.*, 2015; *Mordensky et al.*, 2018].

203 Although pre-eruptive swarms occur consistently on the main ring structure, our re-
 204 sults show a clear correlation between earthquake locations and the azimuth of eruptive
 205 sites relative to the central cone (Fig. 2). In addition, the delay between the seismic crisis
 206 and the eruption onset correlates relatively well with the distance of the eruption fissure
 207 relative to the magma chamber (Fig. 3). To gain further insights into this pre-eruptive ac-
 208 tivity, we also investigate the evolution of earthquake locations during each eruptive un-
 209 rest. Interestingly, we notice a systematic migration of the earthquake activity during the
 210 seismic crises (Fig. 4 and Fig. S5). These seismicity migrations correspond primarily to
 211 an east to west propagation at a speed of the order of 0.1 m.s^{-1} . Westward propagations
 212 are usually associated with an upward seismicity migration at a similar speed (see right
 213 subplots in Fig. 4). This earthquake migration speed is consistent with the overall magma
 214 migration velocity inferred in section 3. Although the horizontal direction of earthquake
 215 migrations is sometimes consistent with eruptive fissure locations (e.g., Fig. 4b), the evo-
 216 lution of seismicity is often not in agreement with the final location of the eruption site
 217 (e.g., Fig. 4a where eruptive fissures are located at the south-east of a westward migrating
 218 swarm).

219 A simple interpretation of these results is that the observed seismicity responds to
 220 blade-like dike intrusions propagating vertically from the roof of the magma reservoir. We
 221 can suppose that only the weakened part of the edifice located close to the intruding dike
 222 will be activated seismically. The upward seismicity migration from east to west could
 223 then be attributed to the eastward dip of the ring structure. Indeed, because of this struc-
 224 ture geometry, an upward migrating stress source will cause the failure of events located
 225 more and more to the west. Once this intruding dike has inflated vertically, its lateral
 226 propagation direction is mostly controlled by its location relative to the volcano summit
 227 (i.e. the stress field created by the topography) and the existence of preferential intrusion
 228 paths [e.g., rift zones; *Michon et al.*, 2015]. This interpretation is consistent with the anal-
 229 ysis of geodetic time-series that evidenced two phases of dike propagation: first a vertical
 230 migration when the magma leaves the reservoir, and then a lateral migration in the direc-
 231 tion of the eruptive site [*Peltier et al.*, 2005, 2007].

Our findings suggest that a careful analysis of the seismicity during the onset of a magma intrusion provides direct information on the future eruption location. More specifically, at a given time after the beginning of a seismic crisis, we can predict the azimuth and minimum distance of the eruptive site relative to the summit area. After a seismically active phase at the beginning of the intrusion, the magma propagates almost aseismically up to the surface. Although seismicity is very low after the seismic crisis, a few events can still be detected during this second phase. This is illustrated in Fig. 4b where a shallow seismicity cluster is activated close to the final eruptive site 40 min before the eruption (cf., black arrow in Fig. 4b). Our tests show that including more stations away from the central cone does not allow to increase the number of detections at shallow depth. This is mainly due to the limited number of templates located out of the ring structure. Shallow events are difficult to locate because they are usually observed only at a few stations with small signal to noise ratio (hence they can't be used as templates in our detection and relocation procedure). The development of a dedicated approach tracking the location of such shallow micro-earthquakes is of major interest at Piton de la Fournaise, where the prediction of the location of an eruption is important to plan rescue and evacuation operations. Some approaches have been proposed to get approximate locations based on time-averaged seismic amplitudes or amplitude ratios [Taisne *et al.*, 2011; De Barros *et al.*, 2013]. Beyond the implications for monitoring purposes, the development of new approaches enabling accurate localization of individual induced micro-earthquakes is important to improve our understanding of the dynamics of magma propagation.

Acknowledgments

This project was supported by the IPGS internal call for projects and the CNRS-INSU Tellus-ALEAS program. This project has also received funding from the European Research Council (ERC, under the European Union's Horizon 2020 research and innovation programme under grant agreement No 805256) and from Agence Nationale de la Recherche (project ANR-17-ERC3-0010). We thank Patrice Boissier, Aline Peltier, Benoit Taisne and Michael Heap for helpful discussions. Michel Tas is additionally thanked for grammatical assistance. We thank the Editor, Rebecca Carey, and two anonymous reviewers for their constructive comments, which helped improve this manuscript. The data used in this study, were acquired by the Volcanological and Seismological Observatory of Piton de la Fournaise (OVPF - IPGP) and is accessible via the VOLOBSIS Portal at

264 http://volobsis.ipgp.fr. Figures were made with the GMT software [Wessel and Smith,
 265 2006]

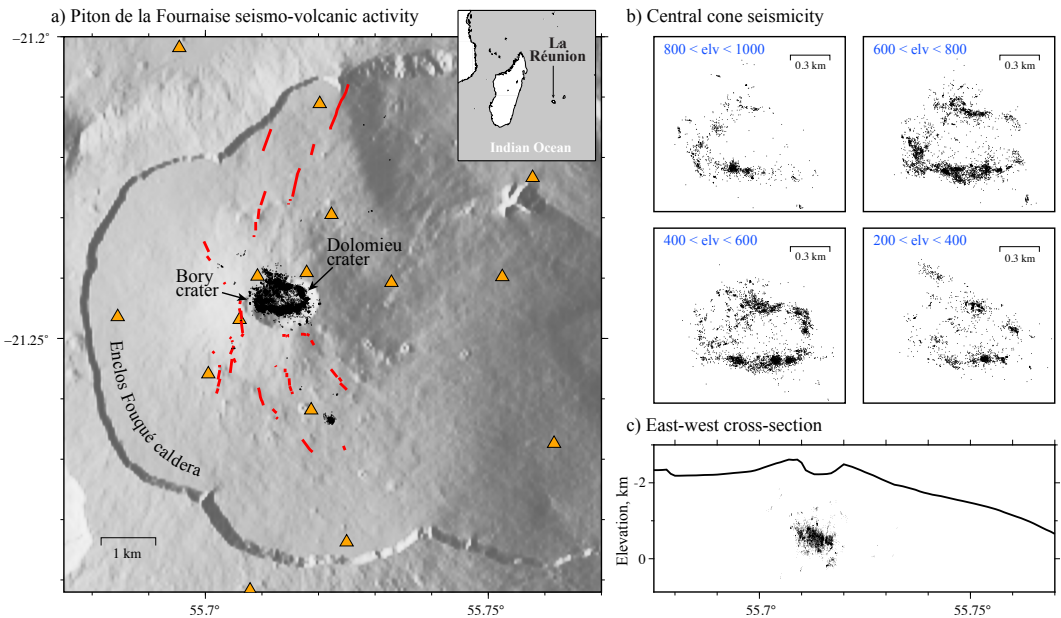
266 **References**

- 267 Aki, K., and V. Ferrazzini (2000), Seismic monitoring and modeling of an active volcano
 268 for prediction (vol 105, pg 16,617, 2000), *J. Geophys. Res.*, *105*(B10), 23,763–23,763.
- 269 Aki, K., and R. Koyanagi (1981), Deep volcanic tremor and magma ascent mechanism
 270 under Kilauea, Hawaii, *J. Geophys. Res.*, *86*(B8), 7095–7109.
- 271 Battaglia, J., V. Ferrazzini, T. Staudacher, K. Aki, and J.-L. Cheminée (2005), Pre-eruptive
 272 migration of earthquakes at the Piton de la Fournaise volcano (Réunion Island), *161*(2),
 273 549–558.
- 274 Brenguier, F., P. Kowalski, T. Staudacher, V. Ferrazzini, F. Lauret, P. Boissier, P. Catherine,
 275 A. Lemarchand, C. Pequegnat, O. Meric, C. Pardo, A. Peltier, S. Tait, N. M.
 276 Shapiro, M. Campillo, and A. Di Muro (2012), First Results from the UnderVolc High
 277 Resolution Seismic and GPS Network Deployed on Piton de la Fournaise Volcano, *Seis-*
 278 *mol. Res. Lett.*, *83*(1), 97–102.
- 279 Carrier, A., and J. L. Got (2014), A maximum a posteriori probability time-delay estima-
 280 tion for seismic signals, *Geophys. J. Int.*, *198*(3), 1543–1553.
- 281 Carrier, A., J.-L. Got, A. Peltier, V. Ferrazzini, T. Staudacher, P. Kowalski, and P. Boissier
 282 (2015), A damage model for volcanic edifices: Implications for edifice strength, magma
 283 pressure, and eruptive processes, *J. Geophys. Res.: Solid Earth*, *120*(1), 567–583.
- 284 De Barros, L., C. J. Bean, M. Zecevic, F. Brenguier, and A. Peltier (2013), Eruptive frac-
 285 ture location forecasts from high-frequency events on Piton de la Fournaise Volcano,
 286 *Geophys. Res. Lett.*, *40*(17), 4599–4603.
- 287 Eibl, E. P., C. J. Bean, K. S. Vogfjörd, Y. Ying, I. Lokmer, M. Möllhoff, G. S. O'Brien,
 288 and F. Pálsson (2017), Tremor-rich shallow dyke formation followed by silent magma
 289 flow at bárðarbunga in iceland, *Nature Geoscience*, *10*(4), 299.
- 290 Einarsson, P., and B. Brandsdóttir (1980), Seismological evidence for lateral magma intru-
 291 sion during the july 1978 deflation of the krafla volcano in ne-icehind, *J. Geophys. Res.*,
 292 *47*, 160–165.
- 293 Gailler, L.-S., J.-F. Lénat, M. Lambert, G. Levieux, N. Villeneuve, and J. L. Froger
 294 (2009), Gravity structure of Piton de la Fournaise volcano and inferred mass transfer
 295 during the 2007 crisis, *J. Volc. Geoth. Res.*, *184*(1-2), 31–48.

- 296 Grandin, R., E. Jacques, A. Nercessian, A. Ayele, C. Doubre, A. Socquet, D. Keir,
297 M. Kassim, A. Lemarchand, and G. King (2011), Seismicity during lateral dike prop-
298 agation: Insights from new data in the recent Manda Hararo–Dabbahu rifting episode
299 (Afar, Ethiopia), *Geochem. Geophys. Geosyst.*, 12(4), 1–24.
- 300 Harris, A. J. L., N. Villeneuve, A. Di Muro, V. Ferrazzini, A. Peltier, D. Coppola,
301 M. Favalli, P. Bachèlery, J. L. Froger, L. Gurioli, S. Moune, I. Vlastélic, B. Galle, and
302 S. Arellano (2017), Effusive crises at Piton de la Fournaise 2014–2015: a review of a
303 multi-national response model, *J Appl. Volcanol.*, 6(1), 11.
- 304 Heap, M. J., B. M. Kennedy, N. Pernin, L. Jacquemard, P. Baud, J. I. Farquhar-
305 son, B. Scheu, Y. Lavallee, H. A. Gilg, M. Letham-Brake, K. Mayer, A. D. Jolly,
306 T. Reuschle, and D. B. Dingwell (2015), Mechanical behaviour and failure modes in
307 the Whakaari (White Island volcano) hydrothermal system, New Zealand, *Journal of*
308 *Volcanology and Geothermal Research*, 295, 26–42.
- 309 Lénat, J.-F., P. Bachelery, and O. Merle (2012), Anatomy of Piton de la Fournaise volcano
310 (La Réunion, Indian Ocean), *Bull Volcanol.*, 74(9), 1945–1961.
- 311 Lengliné, O., Z. Duputel, and V. Ferrazzini (2016), Uncovering the hidden signature of a
312 magmatic recharge at Piton de la Fournaise volcano using small earthquakes, *Geophys.*
313 *Res. Lett.*, 43(9), 4255–4262.
- 314 Michon, L., A. Di Muro, N. Villeneuve, C. Saint-Marc, P. Fadda, and F. Manta (2013),
315 Explosive activity of the summit cone of Piton de la Fournaise volcano (La Réunion
316 island): A historical and geological review, *J. Volc. Geoth. Res.*, 264, 117–133.
- 317 Michon, L., V. Ferrazzini, A. Di Muro, N. Villeneuve, and V. Famin (2015), Rift zones
318 and magma plumbing system of Piton de la Fournaise volcano: How do they differ
319 from Hawaii and Etna?, *J. Volc. Geoth. Res.*, 303, 112–129.
- 320 Mordensky, S., M. Villeneuve, B. Kennedy, M. Heap, D. Gravley, J. Farquharson, and
321 T. Reuschlé (2018), Physical and mechanical property relationships of a shallow in-
322 trusion and volcanic host rock, pinnacle ridge, mt. ruapehu, new zealand, *Journal of*
323 *Volcanology and Geothermal Research*, 359, 1–20.
- 324 Peltier, A., V. Ferrazzini, T. Staudacher, and P. Bachèlery (2005), Imaging the dynamics
325 of dyke propagation prior to the 2000–2003 flank eruptions at Piton de La Fournaise,
326 Reunion Island, *Geophys. Res. Lett.*, 32(22), L22,302.
- 327 Peltier, A., T. Staudacher, and P. Bachèlery (2007), Constraints on magma transfers and
328 structures involved in the 2003 activity at Piton de La Fournaise from displacement

- 329 data, *J. Geophys. Res.*, 112(B3).
- 330 Peltier, A., T. Staudacher, P. Bachelery, and V. Cayol (2009), Formation of the April 2007
 331 caldera collapse at Piton de La Fournaise volcano: Insights from GPS data, *J. Volc.
 332 Geoth. Res.*, 184(1), 152–163.
- 333 Pola, A., G. Crosta, N. Fusi, V. Barberini, and G. Norini (2012), Influence of alteration on
 334 physical properties of volcanic rocks, *Tectonophysics*, 566, 67–86.
- 335 Roult, G., A. Peltier, B. Taisne, T. Staudacher, V. Ferrazzini, and A. Di Muro (2012), A
 336 new comprehensive classification of the Piton de la Fournaise activity spanning the
 337 1985–2010 period. Search and analysis of short-term precursors from a broad-band seis-
 338 mological station, *J. Volc. Geoth. Res.*, 241-242, 78–104.
- 339 Rubin, A. M., and D. Gillard (1998), Dike-induced earthquakes: Theoretical considera-
 340 tions, *J. Geophys. Res.*, 103(B5), 10,017–10,030.
- 341 Rubin, A. M., D. Gillard, and J.-L. Got (1998), A reinterpretation of seismicity associ-
 342 ated with the January 1983 dike intrusion at Kilauea Volcano, Hawaii, *J. Geophys. Res.:
 343 Solid Earth*, 103(B5), 10,003–10,015.
- 344 Sapin, M., A. Hirn, J.-C. Lépine, and A. Nercessian (1996), Stress, failure and fluid flow
 345 deduced from earthquakes accompanying eruptions at Piton de la Fournaise volcano, *J.
 346 Volc. Geoth. Res.*, 70(3-4), 145–167.
- 347 Sigmundsson, F., A. Hooper, S. Hreinsdóttir, K. S. Vogfjörd, B. G. Ófeigsson, E. R.
 348 Heimisson, S. Dumont, M. Parks, K. Spaans, G. B. Gudmundsson, et al. (2015), Seg-
 349 mented lateral dyke growth in a rifting event at bárðarbunga volcanic system, iceland,
 350 *Nature*, 517(7533), 191.
- 351 Staudacher, T. (2010), Field observations of the 2008 summit eruption at Piton de la Four-
 352 naise (Ile de La Réunion) and implications for the 2007 Dolomieu collapse, *J. Volc.
 353 Geoth. Res.*, 191(1-2), 60–68.
- 354 Staudacher, T., and A. Peltier (2016), Ground Deformation at Piton de la Fournaise, a Re-
 355 view From 20 Years of GNSS Monitoring, in *Active Volcanoes of the Southwest Indian
 356 Ocean*, pp. 251–269, Springer, Berlin, Heidelberg, Berlin, Heidelberg.
- 357 Taisne, B., F. Brenguier, N. M. Shapiro, and V. Ferrazzini (2011), Imaging the dynamics
 358 of magma propagation using radiated seismic intensity, *Geophys. Res. Lett.*, 38(4), –n/a.
- 359 Waldhauser, F. (2000), A Double-Difference Earthquake Location Algorithm: Method and
 360 Application to the Northern Hayward Fault, California, *Bull. Seism. Soc. Am.*, 90(6),
 361 1353–1368.

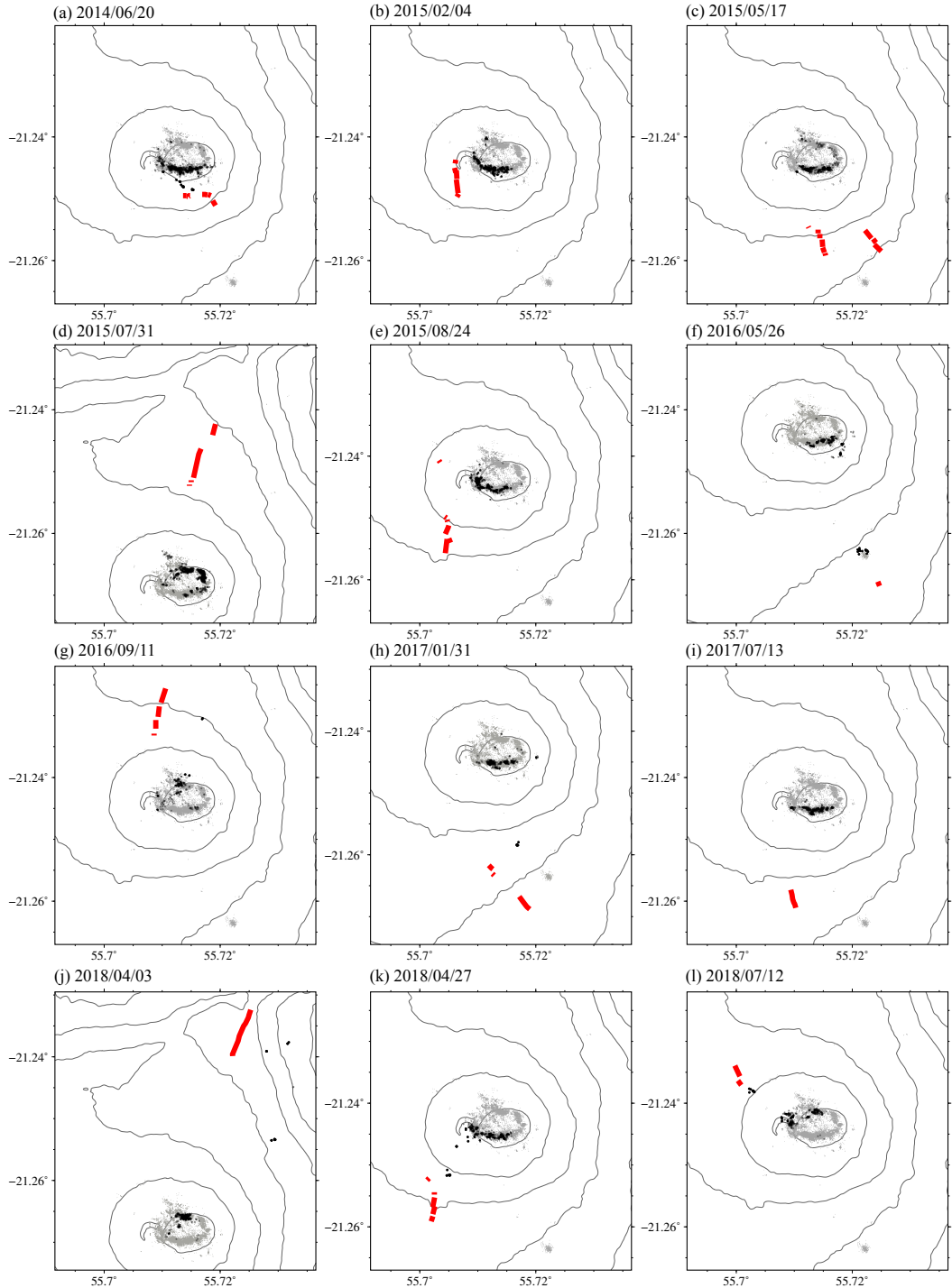
- 362 Wessel, P., and W. H. F. Smith (2006), New, improved version of generic mapping tools
363 released, *Eos Trans. AGU*, 79(47), 579–579.
- 364 Wright, T. J., C. Ebinger, J. Biggs, A. Ayele, G. Yirgu, D. Keir, and A. Stork (2006),
365 Magma-maintained rift segmentation at continental rupture in the 2005 Afar dyking
366 episode, *Nature*, 442(7100), 291–294.
- 367 Wyering, L. D., M. C. Villeneuve, I. C. Wallis, P. A. Siratovich, B. M. Kennedy, D. M.
368 Gravley, and J. L. Cant (2014), Mechanical and physical properties of hydrothermally
369 altered rocks, Taupo Volcanic Zone, New Zealand, *Journal of Volcanology and Geother-
mal Research*, 288, 76–93.
- 370 Zecevic, M., L. De Barros, C. J. Bean, G. S. O'Brien, and F. Brenguier (2013), Investigat-
371 ing the source characteristics of long-period (LP) seismic events recorded on Piton de la
372 Fournaise volcano, La Réunion, *J. Volc. Geoth. Res.*, 258, 1–11.
- 373



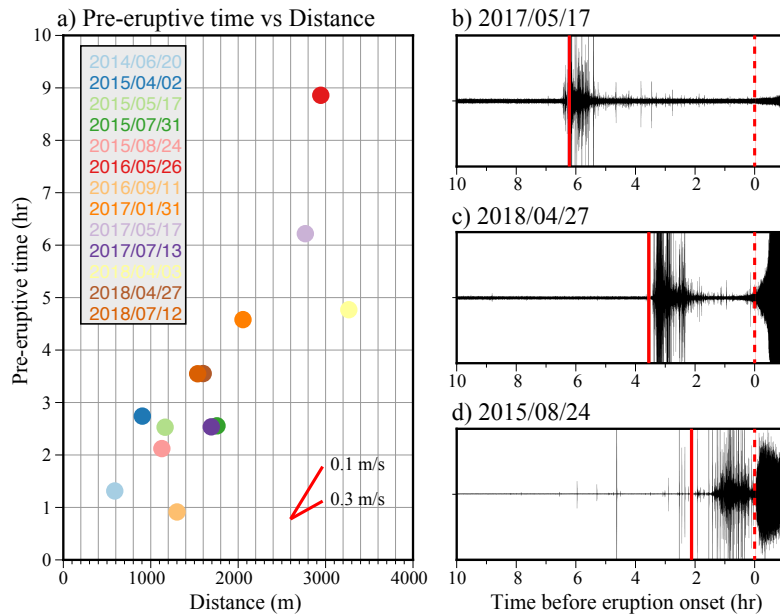
374 **Figure 1.** Relocated earthquake catalog, eruptive fissures and seismic stations. (a) Map view of the 15 598
 375 relocated earthquakes (black circles) and volcanic fissures of eruptions between June 2014 and July
 376 2018 (red lines). Orange triangles indicate seismic stations of the Piton de la Fournaise observatory. (b)
 377 Map view of relocated earthquakes in 4 different depth intervals ("elv" stands for elevation above sea level in
 378 meters). (c) Projection of relocated events onto an East-West cross-section. Topography at latitude -21.45°
 379 is shown for reference. We observe in (b) and (c) that deeper seismicity focuses on the east while shallower
 380 events are mostly located on the west. The overall structure has an eastward dipping angle of $\sim 20^{\circ}$.

Date	Time	Duration	Location
2014/06/20	21:35	19 hours	Summit area
2015/02/04	07:00	11.5 days	Summit area
2015/05/17	09:45	13.3 days	South-east flank
2015/07/31	05:20	2.1 days	North flank
2015/08/24	14:50	58.3 days	South-west flank
2016/05/26	04:05	26 hours	South flank
2016/09/11	04:41	6.8 days	North flank
2017/01/31	15:40	27.0 days	South flank
2017/05/17	16:10 ^a	4.0 days	North flank
2017/07/13	20:50	45.1 days	South flank
2018/04/03	06:40	17 hours	North flank
2018/04/27	19:50	34.6 days	South-west flank
2018/07/12	23:30	19 hours	North-west flank

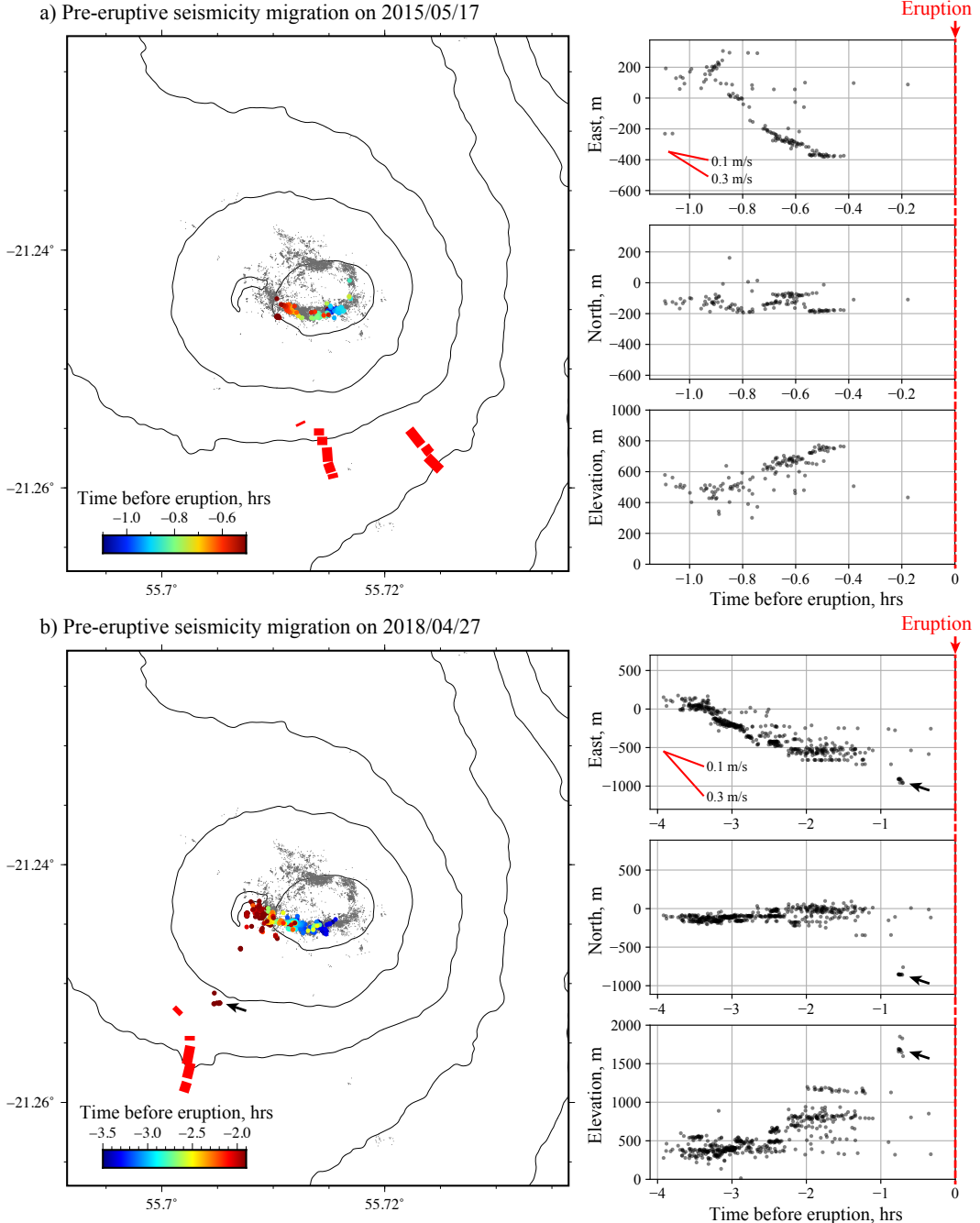
³⁸¹ **Table 1.** Date, time, duration and location of the analyzed eruptions. Eruptive fissures are mapped in Fig. 1,
³⁸² Fig. 2 and Fig. S3. ^a Only gas and no magma was associated with the eruption on 2017/05/17.



383 **Figure 2.** Location of earthquakes and eruptive fissures. Each map presents the seismic crisis preceding
 384 an eruption (cf., date indicated on top of each sub-figure). The location of eruptive fissures is indicated in
 385 red. Black circles represent the seismic events that occurred within 24 hours before the eruption. Grey circles
 386 represent the entire set of relocated seismic events. Fissure locations are based on visual inspections from
 387 field investigations with GPS tracking and photogrammetry. The same map is presented in Fig. S3 for the
 388 eruption of 2017/05/17 that was only associated with gas emissions (no lava was ejected from the fissure). We
 389 also compare the azimuthal distribution of earthquakes and eruptive fissures in Fig. S4.



390 **Figure 3.** Time evolution of pre-eruptive seismic crises. (a) Pre-eruptive swarm time-delay as a function of
 391 distance between earthquakes and eruptive fissures. The pre-eruptive time corresponds to the time difference
 392 between the swarm onset and the eruption onset. (b), (c) and (d) Examples of continuous seismograms on the
 393 vertical component recorded before three eruptions at station BOR, located on the south-west rim of the Bory
 394 crater (cf., Fig. 1). The continuous red line refers to the seismic crisis onset. The dashed red line at time 0
 395 indicates the start of the eruption.



396 **Figure 4.** Pre-eruptive earthquake migrations. (a) Migration observed before the 2015/05/17
 397 eruption. (b) Migration observed before the eruption on 2018/04/27. Earthquakes are color-coded as a
 398 function of time before eruption in the map showed on the left. Sub-figures on the right depict earthquake
 399 coordinates as a function of time. Black arrows in (b) indicate a shallow cluster of seismicity that occurred
 400 close to eruptive fissures about 40 min before the eruption on 2018/04/27. Similar maps are presented in Fig.
 401 S3 of the supporting information for the 11 other eruptions analyzed in this study.